Published in final edited form as:

J Phys Chem C Nanomater Interfaces. 2019 May 9; 123(18): 11734–11744. doi:10.1021/acs.jpcc.9b01538.

Relaxation Dynamics of Nuclear Long-Lived Spin States in Propane and Propane-d_6 Hyperpolarized by Parahydrogen

Nuwandi M. Ariyasingha[a], **Oleg G. Salnikov**[b,c], **Kirill V. Kovtunov**[b,c], **Larisa M. Kovtunova**[c,d], **Valerii I. Bukhtiyarov**[c,d], **Boyd M. Goodson**[e], **Matthew S. Rosen**[f], **Igor V. Koptyug**[b,c], **Juri G. Gelovani**[a], **Eduard Y. Chekmenev**[a,g,*]

[a]Department of Chemistry, Integrative Biosciences (Ibio), Wayne State University, Karmanos Cancer Institute (KCI), Detroit, Michigan, 48202, United States

[b]International Tomography Center SB RAS, 3A Institutskaya St., Novosibirsk, 630090, Russia

[c]Novosibirsk State University, 2 Pirogova St., Novosibirsk, 630090, Russia

[d]Boreskov Institute of Catalysis SB RAS, 5 Acad. Lavrentiev Pr., Novosibirsk, 630090, Russia

[e]Department of Chemistry and Biochemistry and Materials Technology Center, Southern Illinois University, Carbondale, Illinois 62901, United States

[f]Massachusetts General Hospital/Athinoula A. Martinos Center for Biomedical Imaging, Boston, Massachusetts 02129, United States

[g]Russian Academy of Sciences, Leninskiy Prospekt 14, Moscow, 119991, Russia

Abstract

We report a systematic study of relaxation dynamics of hyperpolarized (HP) propane and HP propane-d_6 prepared by heterogeneous pairwise parahydrogen addition to propylene and propylene-d_6 respectively. Long-lived spin states (LLS) created for these molecules at the low magnetic field of 0.0475 T were employed for this study. The parahydrogen-induced overpopulation of a HP propane LLS decays exponentially with time constant (T_{LLS}) approximately 3-fold greater than the corresponding T_1 values. Both T_{LLS} and T_1 increase linearly with propane pressure in the range from 1 atm (the most biomedically relevant conditions for pulmonary MRI) to 5 atm. The T_{LLS} value of HP propane gas at 1 atm is ~3 s. Deuteration of the substrate (propylene-d_6) yields hyperpolarized propane-d_6 gas with T_{LLS} values approximately 20% shorter than those of hyperpolarized fully protonated propane gas, indicating that deuteration does not benefit the lifetime of the LLS HP state. The use of pH_2 or Xe/N_2 buffering gas during heterogeneous hydrogenation reaction (leading to production of 100% HP propane (no buffering gas) versus 43% HP propane gas (with 57% buffering gas) composition mixtures) results in (i) no significant changes in T_1, (ii) decrease of T_{LLS} values (by 35±7% and 8±7% respectively); and (iii) an increase of the polarization levels of HP propane gas with a propane concentration decrease

[*]**Corresponding Author** chekmenev@wayne.edu.

ASSOCIATED CONTENT

Supporting Information.

The following files are available free of charge.

Additional experimental details. Additional figures and Table. (file type, PDF)

(by 1.6±0.1-fold and 1.4±0.1-fold respectively despite the decrease in T_{LLS}, which leads to disproportionately greater polarization losses during HP gas transport). Moreover, we demonstrate the feasibility of HP propane cryo-collection (which can be potentially useful for preparing larger amounts of concentrated HP propane, when buffering gas is employed), and T_{LLS} of liquefied HP propane reaches 14.7 seconds, which is greater than the T_{LLS} value of HP propane gas at any pressure studied. Finally, we have explored the utility of using a partial Spin-Lock Induced Crossing (SLIC) radio frequency (RF) pulse sequence for converting the overpopulated LLS into observable ^{1}H nuclear magnetization at low magnetic field. We find that (i) the bulk of the overpopulated LLS is retained even when the optimal or near-optimal values of SLIC pulse duration are employed, and (ii) the overpopulated LLS of propane is also relatively immune to strong RF pulses—thereby, indicating that LLS is highly suitable as a spin-polarization reservoir in the context of NMR/MRI detection applications. The presented findings may be useful for improving the levels of polarization of HP propane produced by HET-PHIP via the use of an inert buffer gas; increasing the lifetime of the HP state during preparation and storage; and developing efficient approaches for ultrafast MR imaging of HP propane in the context of biomedical applications of HP propane gas, including its potential use as an inhalable contrast agent.

Graphical Abstract

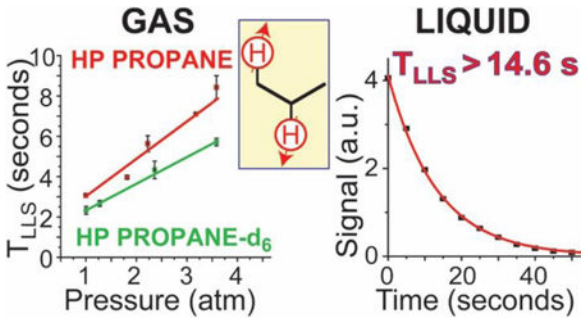

INTRODUCTION

Hyperpolarization increases the nuclear spin polarization by several orders of magnitude over its thermal equilibrium value.[1–2] This dramatic polarization increase results in corresponding gains in NMR and MRI signals.[3–4] Biomedical use of hyperpolarized (HP) spin states enables a variety of new applications, such as probing metabolism and organ function on the time scale of tens of seconds.[1, 5–6] In the case of gases and lung MRI, the potential of HP noble gases like ^{3}He and ^{129}Xe for such applications was demonstrated over 20 years ago,[7–10] and they have been shown safe in clinical trials (e.g. Ref. #[11]). Although HP ^{3}He MRI was demonstrated before ^{129}Xe,[12–14] the supply of ^{3}He is limited (it is a product of tritium decay), thus presenting a significant obstacle to a sustainable widespread clinical use. As a consequence ^{129}Xe is the leading HP noble gas for prospective use as an inhalable contrast agent for imaging COPD,[15] emphysema,[16–17] brown fat,[18] and other applications.[19–21] However, while progress has been made, the clinical-scale hyperpolarization hardware for HP ^{129}Xe preparation remains relatively complex and costly.[12, 22–27] More importantly, clinical MRI scanners are not equipped with the hardware or software required for HP ^{129}Xe imaging, because they are designed to image the ^{1}H spins

from water and lipids in the body, whereas ^{129}Xe resonates at a frequency that is several-fold lower than that of ^{1}H. Due to the above limitations of HP ^{129}Xe production and imaging technologies, the search for biomedically useful inhalable HP contrast agents remains an active area of basic and translational research.

HP gaseous hydrocarbons potentially obviate the shortcomings of HP ^{129}Xe in the context of biomedical applications, because protons of hydrocarbons can be hyperpolarized quickly and cheaply via the parahydrogen utilization.[28–30] Using heterogeneous catalysts, gaseous hydrocarbons can be hyperpolarized via pairwise addition of parahydrogen (pH_2)[6, 31–35] to a suitable unsaturated substrate via a process termed heterogeneous parahydrogen-induced polarization (HET-PHIP). Although gas-phase proton T_1 values are generally short—*ca.* 1 second at 1 atm[36]—a number of approaches have been developed to extend the lifetime of HP states in hydrocarbons, including the use of high operating pressure[36] and reversible dissolution.[37] Most importantly, the pioneering works of Levitt,[38–41] Bodenhausen,[42–43] Warren[44–45] and others[46–49] have demonstrated that the relaxation decay of HP state can be significantly prolonged when two HP nuclear spins are entangled in a singlet state. More broadly in spin systems with three[50] and more spins,[41] long-lived spin states (LLS) can exist due to the symmetry properties of the spin Hamiltonian. The exponential decay constant of LLS T_{LLS} can significantly (by up to several orders of magnitude) exceed T_1.

HP propane has garnered our attention because it is relatively inert,[51–52] has low *in vivo* toxicity,[53] and it is approved by the FDA for the use in the food industry as a propellant and for food storage.[54] More broadly, it is used as a food additive (E944). Therefore, we envision its potential use as an inhalable HP gas in a manner similar to that of HP ^{129}Xe. However, unlike HP ^{129}Xe, HP propane can be produced using relatively simple, low-cost, and high-throughput hyperpolarization hardware,[55] and HP propane can be readily imaged using conventional clinical MRI scanners which can readily detect HP protons of propane gas, [56–59] representing clear advantages for biomedical use. Recently, we have demonstrated a clinical-scale hyperpolarization process for production of pure (from catalyst) HP propane gas capable of producing ~0.3 standard liters of HP hydrocarbon gas in ~2 seconds.[55] As a result, access to HP propane for potential use in humans and large animals is enabled. The work presented here is focused on systematic relaxation studies of HP propane in the gas and liquid states with the key focus on the biomedical application of this potential inhalable contrast agent and extending the lifetime of HP state as much as possible for potential bioimaging applications.

METHODS

Parahydrogen Generation and Experimental Setup.

Two different NMR spectrometer systems were used in this study: One setup used a dual-channel Kea-2 low-field NMR spectrometer (Magritek, New Zealand) to study HP propane at 0.0475 T (Scheme 1) with a previously built radio-frequency (RF) coil.[60] The other setup employed a bench-top 1.4 T NMR spectrometer (NMRPro 60, Nanalysis, Canada) (Scheme S1).

Parahydrogen was prepared using a custom-made pH_2 generator using 99.9995% hydrogen (Airgas) producing a pH_2 enrichment fraction of ~87%. During operation pH_2 is produced continuously and collected in a storage chamber (0.5-liter size) prior to its use in the experiments. pH_2 was combined with propylene (Sigma-Aldrich 295663–300G) or propylene-d_6 (99% atom D, Sigma-Aldrich 455687) gas in a mixing chamber[55] to achieve a given desired ratio of the reagents. In some experiments, an additional cylinder containing a buffering gas (extra pH_2 was added or 3:1 Xe/N_2 mixture was added in parallel, Scheme 1). The prepared reaction mixture was then sent through a mass flow controller (MFC) set to approximately 2,000 standard cubic centimeters per minute (sccm) flow rate (unless otherwise stated), and into the reactor.[36] The catalytic reactor (44-cm-long copper tubing with ¼ in. outer diameter, OD) contains ~280 mg of 1% (by weight) Rh/TiO_2 catalyst mixed with 12 g of copper particles (10–40 mesh size, >99.90% purity, Sigma-Aldrich) in the gas-reaction section, Scheme 1. The gas heating and gas cooling sections of the reactor were also filled with 12 g of the copper particles in each section (with Cu particles added for even heat distribution), giving a total of ~36 g of copper particles in this copper tube; the sections were separated into three stages by glass wool. In the first section, the gas mixture is heated using cartridge heaters connected to a PID temperature controller. The second stage is heated similarly but contains the catalyst (with Cu particles added for even heat distribution) to perform substrate hydrogenation with pH_2 (Scheme 2a and Scheme 2d). The third / final section of the reactor is for gas cooling, where a third PID temperature controller / heater / cooling fan combination is employed to regulate the cooling of the gas, which is facilitated by passing it through another ~12 g of Cu particles (Scheme 1). The gas mixture exiting the reactor is then directed to either the 0.0475 T or the 1.4 T NMR system to collect enhanced ^1H NMR spectra of HP propane or propane-d_6. The following scheme was used for the 0.0475 T system. The HP gas exiting the reactor was sent through a valve (#2′) into the small phantom (17.5 mL) located within the RF coil of the 0.0475 T magnet. The flow of the gas is then directed through another valve (#3′) after which the gas is vented to atmosphere (*i.e.* within a hood) via a safety valve operating at 0–60 psi overpressure. The gas inlet and outlet are also connected via a normally-open (NO) valve (#1′) through a bypass connection to enable the gas flow, when the phantom is closed for the gas flow—this way, the production of HP gas remains uninterrupted.

The details of the 1.4 T apparatus are provided in Scheme S1 in Supporting Information (SI). For these experiments, the HP propane gas exiting the reactor system was directed to the bench-top NMR spectrometer. The inlet was connected to the bottom of a standard 5-mm NMR tube. This NMR tube was cut at the bottom, and glued with epoxy to 1/8 in. OD polyethylene tubing. The NMR tube designed in this fashion was placed inside the NMR spectrometer. The top of the NMR tube was connected to a manual valve (via ¼ in. OD Teflon tubing), which was then vented via two manual valves and a safety valve. Here we also employed a bypass between the inlet and the outlet lines of the NMR tube. A receiver gain of 4 dB was used for all the spectra recorded using this 1.4 T NMR spectrometer system. The 1.4 T bench-top NMR spectrometer arrangement was used to directly measure the polarization enhancement values and chemical conversion of HP propane (Figure 1a) under the following experimental conditions: a 1.2:1 mixture of pH_2:propylene was used at a gas flow rate of 2000 sccm at variable reactor temperature. NMR spectra of HP propane

were acquired in two flow regimes: continuous-flow (Figure 1b, under continuous flow) and stopped-flow (Figure 1d, when the flow was terminated). The overpressure was measured using a pressure gauge connected downstream of the NMR tube setup (Scheme S1). These experiments were performed by flowing the HP gas mixture from the exit of the catalytic reactor into the 5 mm NMR tube via the bottom side of the bench top NMR spectrometer (Scheme S1). The gas exiting at the top of the NMR tube was then flowed through manual valves (#1" and #2") to the vent, and the spectrum was recorded under continuous-flow conditions. In a stopped-flow condition, after flowing the gas for at least 20–40 seconds the gas flow was stopped by dialing zero from the MFC and closing the manual valve #2", so the HP propane gas would be trapped (and stopped) throughout the duration of the NMR spectrum acquisition (Figure 1d). The time delay between stopping the gas flow and the NMR acquisition was 0.5–1 s. After the relaxation of hyperpolarization, NMR spectra of stopped-flow thermally polarized propane gas were recorded (an example is shown in Figure 1c). Although the stopped-flow mode exhibited better spectral resolution because the gas-flow artifacts were eliminated, we generally used the continuous-flow mode for data acquisition owing to the less complicated experimental procedure, more reproducible data, and greater HP signals.

For the HP propane condensation, a slightly modified version of the setup shown in Scheme 1 was employed: the phantom inside the RF coil was replaced by a 5 mm NMR tube via a Wye-connector in which the reaction mixture was cryo-cooled inside a dry ice / ethanol bath at a flow rate of 1300 sccm for ~20 s in the Earth's magnetic field. Then the NMR tube was rapidly placed inside the 0.0475 T magnet, and spectra were collected using a RF SLIC pulse (200 ms).

NMR pulse sequences.

Both the filling of the pressurized phantom and the acquisition of NMR spectra were fully automated in Prospa software (Magritek, New Zealand) using a custom-made pulse program and hardware of the pulse-programmable polarizer described previously.[61] This setup was used for most of the experiments reported here to study the effects of varying the refill duration, spin-lock induced crossing (SLIC)[62] pulse duration, etc. All experiments were conducted by first filling the phantom with HP gas, terminating the flow by closing valves #2′ and 3′, and then applying the sequence of RF pulses of interest on the static HP gas mixture (i.e., under stopped-flow conditions, in contrast with our previous work on HP propane, where RF pulses were applied to continuously flowing HP gas[63]) and finally collecting the FID as shown in Scheme 2b, Scheme 2c, and Scheme 2e.

The exponential decay of the long-lived spin state (LLS) in HP propane is characterized by the exponential decay constant T_{LLS},[57] which was measured by varying the relaxation delay time period as shown in Scheme 2b. The corresponding NMR spectrum of HP propane after SLIC is shown in Figure 2a. After the SLIC transformation of the pH_2-induced overpopulation of the LLS (denoted schematically as a singlet in Figure 3a; it should be noted that the spin eigenstates of protonated propane have eight protons, and therefore the resulting spin system is different from the prototypical 'singlet' and 'triplet' states—after pairwise addition of pH_2 singlet (as the two protons belonging to the CH_2 and CH_3 groups

respectively), many collective states of the proton spin system can be populated, and some of these states can be long-lived due to the symmetry properties of the spin Hamiltonian; therefore, strictly speaking, LLS of propane cannot be called a 'singlet' state), the observable magnetization is aligned along the axis of the SLIC irradiation (i.e. x or y axis of the rotating frame, which is a typical approach employed in NMR to describe the effect of RF pulses), and a 90º pulse is applied to align the magnetization of HP propane along the z-axis (i.e. along the applied static magnetic field referred to as z-axis of the rotating frame), Scheme 2c. After these RF-induced transformations, the resulting z-magnetization decays exponentially according to the spin-lattice decay time constant T_1, which is measured by applying a small-angle excitation pulse α (~10º) followed by FID detection, applied several (N) times to observe the decay (as shown in Scheme 2c). Although LLS exists for HP propane-d_6, the application of a SLIC pulse for transformation of LLS into observable magnetization is not required due to the spin-spin coupling of nascent protons with deuterons—see Ref. # [58] for details. As a result, T_{LLS} can be conveniently measured by applying a small-angle excitation pulse (~10º) followed by FID detection, repeated several times to observe the decay (Scheme 2e). The corresponding NMR spectrum of HP propane-d_6 is shown in Figure 2b.

RESULTS AND DISCUSSION

Optimization of SLIC RF Pulse Sequence and Reaction Temperature, and Tests of Reproducibility.

The effects of different experimental conditions toward the HP propane signal intensity induced by the SLIC pulse were tested in order to optimize the pulse parameters and thereby maximize the HP propane signal (Figure 3). All the data were recorded using the 0.0475 T experimental setup (Scheme 1) via the sequence shown in Scheme 2b. A 1:1 gas mixture of pH_2 and propylene was used for the temperature variation experiments in order to determine the optimal temperature for the reactor, particularly in stage two of the hyperpolarizer setup. The gas flow rate was 2000 sccm, and the refill time was 5 s for each run. For refilling the phantom, first the gas was allowed to flow through the phantom for ~5 seconds with valve #1′ closed and valves #2′ and #3′ open, and after ~5 seconds of gas flow valves #2′ and 3′ were closed, and the bypass valve #1′ was opened. First, the consistency of the HP propane signal was tested (Figure 3b) using a SLIC pulse duration of 500 ms; over numerous scans a standard deviation of ~9% was found, indicating good shot-to-shot reproducibility for the hyperpolarizer. Next, the SLIC sequence was used for the experiment, and three HP propane spectra were collected at each reaction temperature (recorded as the temperature of the reactor's aluminum jacket). The average signal value and the corresponding standard deviation are plotted for each temperature in Figure 3c. The strength of the SLIC RF pulse also has a negligible effect on the signal, as identified in previous studies.[63] Results from SLIC pulse power optimization are shown in Figure 3d; from this SLIC power plot, the highest SLIC signal corresponds to a power setting of −51.25 dB (this value likely corresponds to 20–30 Hz of B_1 power[63]), and this optimal power was used for the remaining studies using the SLIC sequence. The SLIC pulse duration was varied from 2 to 1802 ms, and the signal was found to increase with the SLIC pulse duration and was well-reproduced by a sinusoidal function (in a manner similar to the B_1 nutation curve, which is

predicted by the similar works of Rosen and co-workers,[62] and the previous study of the HP propane system;[63] note that data acquisition at long SLIC times is impractical due to T_2 relaxation effects[63]) (Figure 3e), yielding a SLIC period (t_{SLIC}) of 4.0±0.2 s.[62] The last parameter optimized was the SLIC pulse frequency offset.[63] The offset was swept from ~10 Hz to 80 Hz while monitoring the signal strength, and the resulting signal intensity data indicated an optimal offset of ~45 Hz for the system under study (Figure 3f) using the experimental setup presented here.

^{1}H Relaxation Dynamics of HP Propane at 0.0475 T.

First, we measured T_1 and T_{LLS} values for HP propane gas in the pressure range between 1 and 4.6 atm formed using a 1:1 mixture of pH_2 and propylene at 75 °C and 2000 sccm flow rate. As discussed below, the chemical conversion was ~100% at these conditions, i.e. yielding a nearly 100% propane gas product. We note that a previous T_1 and T_{LLS} study of HP propane[63] was performed within a significantly higher pressure regime (3–7.6 atm total pressure), whereas the present study is focused on a lower pressure regime relevant for the future *in vivo* studies (wherein the gas would need to be imaged at 1 atm). In the overlapping range of the pressure values, the present results generally agree with those of the previous study:[63] although the T_1 and T_{LLS} values reported here are somewhat larger (by approximately 10%), this difference likely reflects the fact that the previous study employed reaction conditions where the chemical conversion of substrates was incomplete. The examples of the signal decay curves associated with T_1 and T_{LLS} of HP propane are shown in Figure 4a and Figure 4c respectively. Figure 4b shows the dependence of HP propane T_1 time on the propane pressure, yielding values in the range of ~1.05 seconds (at 1.6 atm) to 3.4 seconds (at 4.5 atm). Figure 4d shows the corresponding dependence of HP propane T_{LLS} time on the propane pressure, showing values in the range of ~3.1 seconds (at 1.0 atm) to 9.4 seconds (at 4.5 atm). On average, the T_{LLS} values were approximately 3 times greater than the corresponding T_1 values, with nearly linear dependence on pressure, which is in accord with the previous report.[63] Such a linear T_1 dependence is consistent with the major contribution of the gas-phase nuclear spin relaxation being from the spin-rotation mechanism in the intermediate-density (here, multi-amagat) regime.[64–65] Under such conditions, different relaxation times for T_1 and T_{LSS} (and slopes with respect to density) would not be surprising as spin states with different symmetries would likely couple to different rotational states.[64] Future theoretical studies are certainly warranted to provide a more-detailed understanding of the observed trends.

Effect of HP Propane Deuteration on LLS Decay at 0.0475 T.

Since T_{LLS} is considerably greater than T_1 in HP propane, the LLS of HP propane may be better suited for *in vivo* experiments, which would likely require at least several seconds of HP gas handling for inhalation and MR imaging. Given the desire to further lengthen the lifetime of the non-equilibrium spin order endowed by hyperpolarization,[66–67] we also studied the effect of deuteration on T_{LLS} in HP propane-d_6 (the corresponding effective T_1 data is shown in Figure S3), acquiring data under conditions similar to the HP propane T_{LLS} measurements discussed above (Figure 4c). We note that the symmetry of nascent parahydrogen protons is broken in propane-d_6 in a way that the magnetization is already observable, even in the absence of significant chemical shift differences (Figure 2b) at

0.0475; for additional details the reader is referred to Ref. # [58]. Therefore, the data acquisition for HP propane-d_6 was performed differently from that for HP propane (i.e. using the sequence shown in Scheme 2e), and small tipping-angle (~10°) RF excitation pulses followed by NMR signal detection were employed. An example of LLS decay of HP propane-d_6 is shown in Figure 4e. Such T_{LLS} values were plotted against the gas pressure and a linear fit was performed for the data obtained (Figure 4f). According to Figure 4f, T_{LLS} for propane-d_6 increases linearly with pressure, with T_{LLS} values being ~20% lower (on average) than the corresponding T_{LLS} values of HP propane (Figure 4d). We note that this small difference is likely a combination of two effects: some depolarization losses due to RF excitation pulses (not taken into account) employed for data collection for HP propane-d_6, as well as the effect of deuterium labeling of the substrate; future theoretical studies are certainly warranted to provide the understanding of the observed trends. Taking into account the RF pulse excitation (which we did not perform due to concerns described by Kharkov and co-workers[68]) would lengthen T_{LLS} values by less than 8%, which is insufficient to account for the ~20% difference between T_{LLS} values of HP propane and HP propane-d_6. We also note a different slope of the curves shown in Figures 4d and 4f.

It should be noted that although HP propane-d_6 T_{LLS} values are generally lower than the corresponding values for HP propane, the detection of HP propane-d_6 offers an advantage of direct detection using a hard, short RF excitation pulse, whereas a long soft SLIC pulse is required to obtain observable magnetization in case of using HP propane at low magnetic fields. This advantage can be useful in the context of MRI applications, because RF excitation pulses can be very short (compared to SLIC RF pulses).

NMR Spectroscopy of HP Propane Gas at 1.4 T.

We note that the methylene and methyl proton resonances still partially overlap at 1.4 T; the spectral appearance was well-reproduced by spectral simulation. No traces of unreacted propylene were seen (monitored by the lack of methine proton resonances after multiple averaging, data not shown) consistent with a full (i.e. near 100%) chemical conversion of the unsaturated substrate in the hydrogenation reaction with pH_2 under these experimental conditions: a corresponding NMR spectrum of thermally polarized propylene is provided in Figure S2.

We note that SLIC-based detection does not allow obtaining the true value of polarization enhancement of the overpopulated LLS at 0.0475 T,[63] because SLIC transformation does not offer a 100% conversion efficiency of the LLS into observable magnetization. On the other hand, direct detection of HP propane gas at 1.4 T was employed to measure polarization enhancement values. For this purpose, the integral values of the signals from H_A and H_B protons (the continuous-flow mode) (Figure 1, we note that the absolute values for H_A and H_B were similar) were compared to the corresponding integral values for thermally polarized propane under the same pressure and multiplied by a factor of 8 (to account for eight protons contributing to the NMR signal of thermally polarized propane). The enhancement values recorded in such manner for the H_A proton were nearly unchanged (ε_{HA} ranging from 950 to 1150, Figure 1e) over the range of reactor temperatures studied (between 20 °C to 140 °C), in agreement with our similar studies using the 0.0475 T setup

(Figure 3a). This trend is important for two reasons. First of all, it indicates that a robust catalyst performance in production of HP propane gas can indeed be obtained over a wide range of temperatures with effectively ~100% chemical conversion (note: 20% excess pH_2 was employed for data collection in Figure 1e). Second, the highest levels of polarization enhancement were observed at 40–60 °C, suggesting that reactor temperatures near that of the human body (ca. 40 °C) can be readily employed without sacrificing polarization efficiency. This finding bodes well for future *in vivo* use of HP propane gas, because the produced HP propane can be immediately inhaled by the subject without the need for significant additional cooling.

Effects of Buffering Gases on Propane Hyperpolarization Level and Decay.

The effect of the buffering gas on the relaxation constants and polarization values of HP propane was also studied using the 0.0475 T NMR spectrometer setup (Scheme 1). For these experiments, we used a flow rate of 2000 sccm, a reaction temperature of 75 °C, and 38 psi overpressure (total pressure of 3.6 atm); SLIC sequences were used for all acquisitions. The results obtained with pH_2 buffering gas and with variable propane concentrations are shown in Figures 5a, 5b and 5c, whereas those obtained with Xe/N_2 mixture (3:1 ratio) as the buffering gas and with variable propane concentration are shown in Figures 5d, 5e, and 5f. The rationale for the mixture of Xe and N_2 was to test the effects of a reduced gas diffusion by using a dense gas (indeed, we note that previous attempts employing pure Xe were challenging because of high gas viscosity). The results indicate that T_1 decay of HP propane is not significantly impacted by the presence of light (H_2) or heavy (Xe/N_2) buffering gases, as shown in Figures 5a and 5d respectively. However, LLS decay of HP propane decreases significantly (by 35±7% from 100% to 43% mixture) with the increased presence of a light buffering gas, H_2 (Figure 5b). Yet in the presence of a heavy buffering gas (Xe/N_2, 3/1), the observed decrease in T_{LLS} is far more modest (by 8±7% from 100% to 43% mixture, Figure 5e). Note, if we consider polarization levels, pH_2 is not truly a buffering gas, because its concentration can influence the processes occurring on the catalyst surface including the percentage of pairwise hydrogen addition. On the other hand, Xe/N_2 mixture is inert relative to the catalyst operation (except the dilution of the reactants leading to decrease of their partial pressures). The ^1H polarization values increase in the presence of the buffering gas by 1.6±0.1 fold (100% propane mixture versus 43% propane mixture) in case of H_2 buffering gas (in agreement with previous studies[36, 69]), and by 1.4±0.1 fold (100% propane mixture versus 43% propane mixture) in case of Xe/N_2 (3:1) buffering gas, as shown in Figures 5c and 5f respectively. We note that the actual increase in (initial) polarization of HP propane gas may be significantly greater, because in the case of more dilute mixtures, HP propane has lower corresponding T_{LLS} values (see Figures 5c and 5f), and therefore, likely experiences disproportionately greater polarization losses during more than 5–10-second transport time from the reactor to the detector.

The observation that the buffering gas boosts propane hyperpolarization in HET PHIP process is important in the context of biomedical applications with the goal of maximizing the levels of hyperpolarization. Although the produced HP gas is diluted with the buffering gas, it can potentially be separated by rapid cryo-condensation of HP propane gas, as discussed below.

Partial SLIC RF excitation of HP propane gas at 0.0475 T.

We carried out a series of experiments with a variable SLIC pulse duration on HP propane gas using the 0.0475 T spectrometer setup (Scheme 1) for a 1:1 reaction mixture of propylene and pH_2 at 38 psi overpressure (~3.6 atm total pressure). Once the phantom was filled with fresh HP propane gas, the SLIC pulse was applied followed by immediate signal detection, and these two steps were repeated for N times on a single fill of HP propane (Figure 6a). The signal of HP propane obtained in this fashion falls exponentially as a result of a combination of LLS decay and the application of SLIC pulses. Several different SLIC RF pulse durations (varying between 50 and 1600 ms) were employed to record NMR spectra, the intensities of which are plotted against time in Figure 6b. We note that in case of longer SLIC durations, the RF pulses were applied more sparsely, resulting in a longer repetition time (TR) but in greater signal intensities (Figure 6c). An effective T_{LLS} value was determined for each experimental series in Figure 6b, and these effective T_{LLS} values (detailed in Table S1) are plotted in Figure 6d. As expected, when the SLIC pulse duration is increased, the effective decay time constant decreases, indicating a faster depleting of the HP state. All effective T_{LLS} values measured in this fashion were in the range of 4.7 s to 8.1 s (due to decay and RF depletion), which is less than the corresponding T_{LLS} value (~8.4 s) obtained at otherwise-identical conditions using the procedure described above (*cf.* Figure 4d). This finding indicates that partial SLIC can be applied to HP propane to convert only a fraction of the hyperpolarization pool at one time (prolonging the useful lifetime of the enhanced spin order). We note that even though near-optimal values of SLIC pulses are applied (i.e. 800–1600 ms durations, making an analogy with a 90° excitation pulse—note the corresponding signal produced by SLIC pulse increases with duration, Figure 3e and Figure 6c), the overpopulated LLS remains largely intact, because subsequent RF excitation pulses produce comparable signal levels, Figure 6a. This finding is useful for several reasons. First, a short SLIC pulse (i.e., with the duration significantly shorter than the optimal value) can be employed in a manner similar to a small tipping-angle excitation pulse for applications ranging from measurements of relaxation of HP species to MRI encoding. In case of MRI applications, we note that the resulting magnetization (after SLIC pulse) is in the x-y plane, and therefore, can be conveniently combined with echo-planar imaging (EPI) readout. As a result, SLIC can provide both partial excitation of overpopulated LLS to record 2D slices, and also enable singlet order selection (SOS) filtering[70] for selective excitation of the singlet states in the presence of proton background signal of tissues.

There are at least two possible explanations for the observed retention of overpopulated LLS even after the application of a SLIC pulse of optimal duration (which in principle is designed to convert all singlet order into observable magnetization[62]). First, gas convection and B_1 inhomogeneities may lead to subpar performance of the SLIC pulse sequence, leaving the bulk of the HP LLS unaffected by the SLIC pulse sequence.[68] Second, the HP propane spin system cannot be, strictly speaking, treated as a true singlet,[57–58, 63] because there are eight spin-spin coupled protons, and therefore, the application of the SLIC sequence may indeed generate observable magnetization while retaining some overpopulated LLS in the spin system of HP propane gas. Future studies using stronger magnets and more homogeneous excitation RF coils are certainly warranted to delineate the relative contribution of these two effects.

We have also tested the immunity of the overpopulated LLS with respect to irradiation by hard RF pulses. The applied sequence is shown in Figure 7a, and the corresponding decay data is presented in Figure 7b (red curve). Specifically, we have employed a SLIC pulse duration of 200 ms, which was followed by signal acquisition. This partial SLIC detection was repeated four times. Next, 64 hard 90° RF pulses were applied back-to-back. This process was repeated three times, and the integral intensity of the HP signals (obtained via partial SLIC and shown as red squares in Figure 7b) is plotted versus time. The resulting data were fit to give an effective T_{LLS} constant of 5.3±0.1 s. This value is close to a corresponding value obtained when no hard RF pulses were employed: effective T_{LLS} of 6.3±0.4 seconds (Figure 7b, blue curve), indicating that the overpopulated LLS is relatively immune to the application of hard RF pulses. This observation is useful in the context of future MR imaging studies, where the application of strong RF pulses may be desirable for background signal suppression, while retaining the overpopulated LLS of HP propane gas.

Feasibility of Condensation of HP Propane Gas and LLS Decay of Liquefied HP Propane at 0.0475 T.

Cryo-collection of HP gas is a common practice in a continuous-flow production of HP noble gases, a practice that is designed to make the contrast agent more concentrated.[26, 71–72] Since the addition of buffering gas increases the degree of propane hyperpolarization (Figure 5c and Figure 5f), we have investigated the feasibility of HP propane cryo-collection. A slight modification to the 0.0475 T experimental setup was made to perform HP propane condensation (Scheme 1 and Methods section for details). The phantom inside the RF coil was replaced by a 5 mm NMR tube wherein the reaction mixture was cryo-cooled. The cryo-cooling was performed at a flow rate of 1300 sccm for ~20 s inside a cooling bath with dry ice and ethanol (*ca.* −78 °C) outside the magnet, i.e. at the Earth's magnetic field. Then the NMR tube containing liquid HP propane was carefully placed inside the magnet, and a series of NMR spectra were collected using partial SLIC excitation with 200 ms pulse duration. The typical NMR spectrum of the liquefied propane (Figure S1a) was similar to the one of HP propane gas (Figure 2a). The fitting to mono-exponential decay (Figures S1b–d) revealed an effective T_{LLS} time constant of 14.7±0.5 s. We note that this value is actually a lower-limit estimate, because the partial SLIC excitation reduces the pool of HP LLS (Table S1), and the effect of the RF pulse-associated losses was not taken into account in our data fitting. Nevertheless, this relatively long T_{LLS} value is significantly greater than any T_{LLS} value of HP propane in the gas phase measured here or elsewhere.[63] This lower-limit T_{LLS} value for liquid HP propane is somewhat lower than the T_1 value of HP propane dissolved in deuterated organic solvents (28–35 s).[37]

Because higher polarization values can be obtained via HET-PHIP using buffering gases, and because buffering gases can be potentially separated from cryo-collected HP propane, this approach may be a viable option for future experimentations to boost propane hyperpolarization via HET-PHIP. Moreover, the relatively long T_{LLS} value of cryo-collected HP propane may be a useful means for temporary storage of HP propane gas prior to its use as an inhalable contrast agent.

CONCLUSION

A systematic study of nuclear spin relaxation dynamics at 0.0475 T of HP propane prepared by HET-PHIP is reported using a clinical-scale hyperpolarizer device under conditions providing nearly 100% chemical conversion. We find that the HP propane T_{LLS} is ~3 seconds at 1 atm, i.e. under clinically relevant conditions. T_{LLS} and T_1 values generally exhibit a linear dependence on propane pressure. At the pressures studied, the T_{LLS} values are approximately 3 times greater than the corresponding T_1 values. The use of deuterated propylene as HP propane precursor (i.e. production of HP propane-d_6) reduces T_{LLS} by as much as ~20%, indicating that deuteration of the precursor maybe somewhat detrimental to the lifetime of the HP state. The use of light and heavy buffering gases (pH_2 and a 3:1 mixture of Xe:N_2) is found to have a negligible effect on T_1 and generally results in somewhat lower T_{LLS} values: the T_{LLS} reduction is concentration dependent. At the same time, the use of buffering gases increases the polarization levels of HP propane gas during HET-PHIP production, which is welcome in the context of biomedical applications. Although the buffering gas dilutes the HP propane gas, it can be separated through a process of HP propane cryo-collection, the feasibility of which was demonstrated here. The added benefit of HP propane cryo-collection is the increase of the T_{LLS} value to 14.7 seconds in the liquid state, which is significantly greater than any reported T_{LLS} value for HP propane gas at any pressure, and which can be useful for temporary storage of produced HP propane prior to its *in vivo* administration. We have also investigated the possibility of applying a partial SLIC pulse to HP propane LLS, and we find that most of the pool of the over-populated LLS is retained even after application of an optimized SLIC pulse. The overpopulated LLS of propane is relatively immune to the application of hard RF pulses. This behavior of the HP propane spin system with respect to application of partial SLIC and strong RF pulses can be potentially useful for developing efficient ultra-fast MR imaging approaches, especially those involving EPI readout. To summarize, the results presented in this study may be beneficial for guiding future work studying the preparation of highly polarized batches of HP propane and designing efficient MR imaging approaches.

Supplementary Material

Refer to Web version on PubMed Central for supplementary material.

ACKNOWLEDGEMENTS

This work was supported by NSF under grant CHE-1836308 and CHE-1416432, NIBIB under 1R21EB020323, DOD CDMRP under W81XWH-15-1-0271 W81XWH-15-1-0272. The Russian team thanks RFBR (projects # 17-54-33037 OHKO_a, 18-43-543023) and the Russian Ministry of Science and Higher Education (AAAA-A16-116121510087-5) for the support.

REFERENCES

1. Goodson BM Nuclear Magnetic Resonance of Laser-Polarized Noble Gases in Molecules, Materials, and Organisms. J. Magn. Reson 2002, 155, 157–216. [PubMed: 12036331]
2. Kovtunov KV; Pokochueva EV; Salnikov OG; Cousin S; Kurzbach D; Vuichoud B; Jannin S; Chekmenev EY; Goodson BM; Barskiy DA; Koptyug IV Hyperpolarized NMR: D-DNP, PHIP, and SABRE. Chem. Asian J 2018, 13, 1857–1871.

3. Albert MS; Cates GD; Driehuys B; Happer W; Saam B; Springer CS; Wishnia A Biological Magnetic-Resonance-Imaging Using Laser Polarized Xe-129. Nature 1994, 370, 199–201. [PubMed: 8028666]
4. Golman K; Axelsson O; Johannesson H; Mansson S; Olofsson C; Petersson JS Parahydrogen-Induced Polarization in Imaging: Subsecond C-13 Angiography. Magn. Reson. Med 2001, 46, 1–5. [PubMed: 11443703]
5. Kurhanewicz J; Vigneron DB; Brindle K; Chekmenev EY; Comment A; Cunningham CH; DeBerardinis RJ; Green GG; Leach MO; Rajan SS; Rizi RR; Ross BD; Warren WS; Malloy CR Analysis of Cancer Metabolism by Imaging Hyperpolarized Nuclei: Prospects for Translation to Clinical Research Neoplasia 2011, 13, 81–97. [PubMed: 21403835]
6. Hövener J-B; Pravdivtsev AN; Kidd B; Bowers CR; Glöggler S; Kovtunov KV; Plaumann M; Katz-Brull R; Buckenmaier K; Jerschow A; Reineri F; Theis T; Shchepin RV; Wagner S; Bhattacharya P; Zacharias NM; Chekmenev EY Parahydrogen-Based Hyperpolarization for Biomedicine. Angew. Chem. Int. Ed 2018, 57, 11140–11162.
7. Bhaskar ND; Happer W; McClelland T Efficiency of Spin Exchange between Rubidium Spins and Xe-129 Nuclei in a Gas. Phys. Rev. Lett 1982, 49, 25–28.
8. Happer W; Miron E; Schaefer S; Schreiber D; Van. Wijngaarden WA; Zeng X Polarization of the Nuclear Spins of Noble-Gas Atoms by Spin Exchange with Optically Pumped Alkali-Metal Atoms. Phys. Rev. A 1984, 29, 3092–3110.
9. Chupp TE; Wagshul ME; Coulter KP; Mcdonald AB; Happer W Polarized, High-Density, Gaseous He 3 Targets. Phys. Rev. C 1987, 36, 2244–2251.
10. Cates GD; Benton DR; Gatzke M; Happer W; Hasson KC; Newbury NR Laser Production of Large Nuclear-Spin Polarization in Frozen Xenon. Phys. Rev. Lett 1990, 65, 2591–2594. [PubMed: 10042636]
11. Driehuys B; Martinez-Jimenez S; Cleveland ZI; Metz GM; Beaver DM; Nouls JC; Kaushik SS; Firszt R; Willis C; Kelly KT; Wolber J; Kraft M; McAdams HP Chronic Obstructive Pulmonary Disease: Safety and Tolerability of Hyperpolarized Xe-129 MR Imaging in Healthy Volunteers and Patients. Radiology 2012, 262, 279–289. [PubMed: 22056683]
12. Walker TG; Happer W Spin-Exchange Optical Pumping of Noble-Gas Nuclei. Rev. Mod. Phys 1997, 69, 629–642.
13. Ebert M; Grossmann T; Heil W; Otten WE; Surkau R; Leduc M; Bachert P; Knopp MV; Schad LR; Thelen M Nuclear Magnetic Resonance Imaging with Hyperpolarised Helium-3. Lanclet 1996, 11, 9011.
14. Kauczor HU; Hofmann D; Kreitner KF; Nilgens H; Surkau R; Heil W; Potthast A; Knopp MV; Otten EW; Thelen M Normal and Abnormal Pulmonary Ventilation: Visualization at Hyperpolarized He-3 MR Imaging. Radiology 1996, 2, 564–568.
15. Kaushik SS; Cleveland ZI; Cofer GP; Metz G; Beaver D; Nouls J; Kraft M; Auffermann W; Wolber J; McAdams HP; Driehuys B Diffusion-Weighted Hyperpolarized Xe-129 MRI in Healthy Volunteers and Subjects with Chronic Obstructive Pulmonary Disease. Magn. Reson. Med 2011, 65, 1155–1165.
16. Stephen MJ; Emami K; Woodburn JM; Chia E; Kadlecek S; Zhu J; Pickup S; Ishii M; Rizi RR; Rossman M Quantitative Assessment of Lung Ventilation and Microstructure in an Animal Model of Idiopathic Pulmonary Fibrosis Using Hyperpolarized Gas MRI. Acad. Radiol 2010, 17, 1433–1443. [PubMed: 20934126]
17. Mugler JP; Altes TA Hyperpolarized ^{129}Xe MRI of the Human Lung. J. Magn. Reson. Imaging 2013, 37, 313–331. [PubMed: 23355432]
18. Branca RT; He T; Zhang L; Floyd CS; Freeman M; White C; Burant A Detection of Brown Adipose Tissue and Thermogenic Activity in Mice by Hyperpolarized Xenon MRI. Proc. Natl. Acad. Sci. U. S. A 2014, 111, 18001–18006. [PubMed: 25453088]
19. Barskiy DA; Coffey AM; Nikolaou P; Mikhaylov DM; Goodson BM; Branca RT; Lu GJ; Shapiro MG; Telkki V-V; Zhivonitko VV; Koptyug IV; Salnikov OG; Kovtunov KV; Bukhtiyarov VI; Rosen MS; Barlow MJ; Safavi S; Hall IP; Schröder L; Chekmenev EY NMR Hyperpolarization Techniques of Gases. Chem. Eur. J 2017, 23, 725–751. [PubMed: 27711999]

20. Wild JM; Marshall H; Xu X; Norquay G; Parnell SR; Clemence M; Griffiths PD; Parra-Robles J Simultaneous Imaging of Lung Structure and Function with Triple-Nuclear Hybrid MR Imaging. Radiology 2013, 267, 251–255. [PubMed: 23264344]
21. Butler JP; Loring SH; Patz S; Tsuda A; Yablonskiy DA; Mentzer SJ Evidence for Adult Lung Growth in Humans. N. Engl. J. Med 2012, 367, 244–247. [PubMed: 22808959]
22. Zook AL; Adhyaru BB; Bowers CR High Capacity Production of > 65% Spin Polarized Xenon-129 for NMR Spectroscopy and Imaging. J. Magn. Reson 2002, 159, 175–182. [PubMed: 12482697]
23. Ruset IC; Ketel S; Hersman FW Optical Pumping System Design for Large Production of Hyperpolarized Xe-129. Phys. Rev. Lett 2006, 96, 053002. [PubMed: 16486926]
24. Freeman MS; Emami K; Driehuys B Characterizing and Modeling the Efficiency Limits in Large-Scale Production of Hyperpolarized ^{129}Xe. Phys. Rev. A 2014, 90, 023406. [PubMed: 25400489]
25. Nikolaou P; Coffey AM; Walkup LL; Gust BM; Whiting NR; Newton H; Muradyan I; Dabaghyan M; Ranta K; Moroz G; Patz S; Rosen MS; Barlow MJ; Chekmenev EY; Goodson BM Xena: An Automated 'Open-Source' ^{129}Xe Hyperpolarizer for Clinical Use. Magn. Reson. Imaging 2014, 32, 541–550. [PubMed: 24631715]
26. Rosen MS; Chupp TE; Coulter KP; Welsh RC; Swanson SD Polarized Xe-129 Optical Pumping/ Spin Exchange and Delivery System for Magnetic Resonance Spectroscopy and Imaging Studies. Rev. Sci. Instrum 1999, 70, 1546–1552.
27. Walker TG Fundamentals of Spin-Exchange Optical Pumping. J. Phys. Conf. Ser 2011, 294, 012001.
28. Koptyug IV; Kovtunov KV; Burt SR; Anwar MS; Hilty C; Han SI; Pines A; Sagdeev RZ Para-Hydrogen-Induced Polarization in Heterogeneous Hydrogenation Reactions. J. Am. Chem. Soc 2007, 129, 5580–5586. [PubMed: 17408268]
29. Kovtunov KV; Zhivonitko VV; Skovpin IV; Barskiy DA; Koptyug IV Parahydrogen-Induced Polarization in Heterogeneous Catalytic Processes. Top. Curr. Chem 2013, 338, 123–180. [PubMed: 23097028]
30. Kovtunov KV; Zhivonitko VV; Skovpin IV; Barskiy DA; Salnikov OG; Koptyug IV Toward Continuous Production of Catalyst-Free Hyperpolarized Fluids Based on Biphasic and Heterogeneous Hydrogenations with Parahydrogen. J. Phys. Chem. C 2013, 117, 22887–22893.
31. Bowers CR; Weitekamp DP Transformation of Symmetrization Order to Nuclear-Spin Magnetization by Chemical-Reaction and Nuclear-Magnetic-Resonance. Phys. Rev. Lett 1986, 57, 2645–2648. [PubMed: 10033824]
32. Bowers CR; Weitekamp DP Para-Hydrogen and Synthesis Allow Dramatically Enhanced Nuclear Alignment. J. Am. Chem. Soc 1987, 109, 5541–5542.
33. Pravica MG; Weitekamp DP Net NMR Alighnment by Adiabatic Transport of Parahydrogen Addition Products to High Magnetic Field. Chem. Phys. Lett 1988, 145, 255–258.
34. Eisenschmid TC; Kirss RU; Deutsch PP; Hommeltoft SI; Eisenberg R; Bargon J; Lawler RG; Balch AL Para Hydrogen Induced Polarization in Hydrogenation Reactions. J. Am. Chem. Soc 1987, 109, 8089–8091.
35. Salnikov OG; Kovtunov KV; Nikolaou P; Kovtunova LM; Bukhtiyarov VI; Koptyug IV; Chekmenev EY Heterogeneous Parahydrogen Pairwise Addition to Cyclopropane. ChemPhysChem 2018, 19, 2621–2626. [PubMed: 30039565]
36. Barskiy DA; Kovtunov KV; Gerasimov EY; Phipps MA; Salnikov OG; Coffey AM; Kovtunova LM; Prosvirin IP; Bukhtiyarov VI; Koptyug IV; Chekmenev EY 2D Mapping of NMR Signal Enhancement and Relaxation for Heterogeneously Hyperpolarized Propane Gas. J. Phys. Chem. C 2017, 121, 10038–10046.
37. Burueva DB; Romanov AS; Salnikov OG; Zhivonitko VV; Chen Y-W; Barskiy DA; Chekmenev EY; Hwang DW-H; Kovtunov KV; Koptyug IV Extending the Lifetime of Hyperpolarized Propane Gas Via Reversible Dissolution. J. Phys. Chem. C 2017, 121, 4481–4487.
38. Carravetta M; Johannessen OG; Levitt MH Beyond the T_1 Limit: Singlet Nuclear Spin States in Low Magnetic Fields. Phys. Rev. Lett 2004, 92, 153003. [PubMed: 15169282]
39. Carravetta M; Levitt MH Long-Lived Nuclear Spin States in High-Field Solution NMR. J. Am. Chem. Soc 2004, 126, 6228–6229. [PubMed: 15149209]

40. Pileio G; Carravetta M; Levitt MH Storage of Nuclear Magnetization as Long-Lived Singlet Order in Low Magnetic Field. Proc. Natl. Acad. Sci. U. S. A 2010, 107, 17135–17139. [PubMed: 20855584]
41. Levitt MH Symmetry Constraints on Spin Dynamics: Application to Hyperpolarized NMR. J. Magn. Reson 2016, 262, 91–99. [PubMed: 26462592]
42. Vasos PR; Comment A; Sarkar R; Ahuja P; Jannin S; Ansermet J-P; Konter JA; Hautle P; van den Brandt B; Bodenhausen G Long-Lived States to Sustain Hyperpolarized Magnetization. Proc. Natl. Acad. Sci. U. S. A 2009, 106, 18469–18473. [PubMed: 19841270]
43. Ahuja P; Sarkar R; Jannin S; Vasos PR; Bodenhausen G Proton Hyperpolarisation Preserved in Long-Lived States. Chem. Comm 2010, 46, 8192–8194. [PubMed: 20886136]
44. Warren WS; Jenista E; Branca RT; Chen X Increasing Hyperpolarized Spin Lifetimes through True Singlet Eigenstates. Science 2009, 323, 1711–1714. [PubMed: 19325112]
45. Feng Y; Davis RM; Warren WS Accessing Long-Lived Nuclear Singlet States between Chemically Equivalent Spins without Breaking Symmetry. Nature Phys 2012, 8, 831–837. [PubMed: 23505397]
46. Franzoni MB; Buljubasich L; Spiess HW; Munnemann K Long-Lived H-1 Singlet Spin States Originating from Para-Hydrogen in Cs-Symmetric Molecules Stored for Minutes in High Magnetic Fields. J. Am. Chem. Soc 2012, 134, 10393–10396. [PubMed: 22690781]
47. Roy SS; Rayner P; Norcott P; Green GGR; Duckett SB Long-Lived States to Sustain Sabre Hyperpolarised Magnetisation. Phys. Chem. Chem. Phys 2016, 18, 24905–24911. [PubMed: 27711398]
48. Zhou Z; Yu J; Colell JFP; Laasner R; Logan AWJ; Barskiy DA; Shchepin RV; Chekmenev EY; Blum V; Warren WS; Theis T Long-Lived $^{13}C_2$ Nuclear Spin States Hyperpolarized by Parahydrogen in Reversible Exchange at Microtesla Fields. J. Phys. Chem. Lett 2017, 8, 3008–3014. [PubMed: 28594557]
49. Theis T; Ortiz GX; Logan AWJ; Claytor KE; Feng Y; Huhn WP; Blum V; Malcolmson SJ; Chekmenev EY; Wang Q; Warren WS Direct and Cost-Efficient Hyperpolarization of Long-Lived Nuclear Spin States on Universal 15N2-Diazirine Molecular Tags. Sci. Adv 2016, 2, e1501438. [PubMed: 27051867]
50. Dumez J-N; Håkansson P; Mamone S; Meier B; Stevanato G; Hill-Cousins JT; Roy SS; Brown RCD; Pileio G; Levitt MH Theory of Long-Lived Nuclear Spin States in Methyl Groups and Quantum-Rotor Induced Polarisation. J. Chem. Phys 2015, 142, 044506. [PubMed: 25637994]
51. All-Gas-Inc. Propane Gas Properties http://www.allgasinc.com/propane-gas-properties.php.
52. Abdelkhalik A; Askar E; Markus D; Brandes E; El-sayed I; Hassan M; Nour M; Stolz T Explosion Regions of Propane, Isopropanol, Acetone, and Methyl Acetate/Inert Gas/Air Mixtures. J. Loss Prev. Process Ind 2016, 43, 669–675.
53. Stewart RD; Newton PE; Baretta ED; Herrmann AA; Forster HV; Soto RJ Physiological Response to Aerosol Propellants. Environ. Health Perspect 1978, 26, 275–285. [PubMed: 214300]
54. Food and Drug Administration. Code of Federal Regulations Title 21; Office of the Federal Register: United States, 2018; pp 21cfr184.1655.
55. Salnikov OG; Nikolaou P; Ariyasingha NM; Kovtunov KV; Koptyug IV; Chekmenev EY Clinical-Scale Batch-Mode Production of Hyperpolarized Propane Gas for MRI. Anal. Chem 2019, 91, 4741–4746. [PubMed: 30855132]
56. Kovtunov KV; Barskiy DA; Coffey AM; Truong ML; Salnikov OG; Khudorozhkov AK; Inozemtseva EA; Prosvirin IP; Bukhtiyarov VI; Waddell KW; Chekmenev EY; Koptyug IV High-Resolution 3D Proton Hyperpolarized Gas MRI Enabled by Parahydrogen and Rh/TiO_2 Heterogeneous Catalyst. Chem. Eur. J 2014, 20, 11636–11639. [PubMed: 24961814]
57. Kovtunov KV; Truong ML; Barskiy DA; Koptyug IV; Coffey AM; Waddell KW; Chekmenev EY Long-Lived Spin States for Low-Field Hyperpolarized Gas MRI. Chem. Eur. J 2014, 20, 14629–14632. [PubMed: 25263795]
58. Kovtunov KV; Truong ML; Barskiy DA; Salnikov OG; Bukhtiyarov VI; Coffey AM; Waddell KW; Koptyug IV; Chekmenev EY Propane-D_6 Heterogeneously Hyperpolarized by Parahydrogen. J. Phys. Chem. C 2014, 118, 28234–28243.

59. Bouchard LS; Burt SR; Anwar MS; Kovtunov KV; Koptyug IV; Pines A NMR Imaging of Catalytic Hydrogenation in Microreactors with the Use of Para-Hydrogen. Science 2008, 319, 442–445. [PubMed: 18218891]
60. Coffey AM; Truong ML; Chekmenev EY Low-Field MRI Can Be More Sensitive Than High-Field MRI. J. Magn. Reson 2013, 237, 169–174. [PubMed: 24239701]
61. Coffey AM; Shchepin RV; Feng B; Colon RD; Wilkens K; Waddell KW; Chekmenev EY A Pulse Programmable Parahydrogen Polarizer Using a Tunable Electromagnet and Dual Channel NMR Spectrometer. J. Magn. Reson 2017, 284, 115–124. [PubMed: 29028543]
62. DeVience SJ; Walsworth RL; Rosen MS Preparation of Nuclear Spin Singlet States Using Spin-Lock Induced Crossing. Phys. Rev. Lett 2013, 111, 173002-1-5.
63. Barskiy DA; Salnikov OG; Romanov AS; Feldman MA; Coffey AM; Kovtunov KV; Koptyug IV; Chekmenev EY NMR Spin-Lock Induced Crossing (SLIC) Dispersion and Long-Lived Spin States of Gaseous Propane at Low Magnetic Field (0.05 T). J. Magn. Reson 2017, 276, 78–85. [PubMed: 28152435]
64. Lemaire C; Armstrong RL Proton Spin Longitudinal Relaxation Time in Gaseous Ammonia and Hydrogen Chloride. J. Chem. Phys 1984, 81, 1626–1631.
65. True NS Gas Phase Applications of NMR Spectroscopy. In Encyclopedia of Spectroscopy and Spectrometry, Lindon JC, Ed. Elsevier: Oxford, 1999; pp 660–667.
66. Taglang C; Korenchan DE; von Morze C; Yu J; Najac C; Wang S; Blecha JE; Subramaniam S; Bok R; VanBrocklin HF; Vigneron DB; Ronen SM; Sriram R; Kurhanewicz J; Wilson DM; Flavell RR Late-Stage Deuteration of ^{13}C-Enriched Substrates for T_1 Prolongation in Hyperpolarized ^{13}C MRI. Chem. Comm 2018, 54, 5233–5236. [PubMed: 29726563]
67. Shchepin RV; Coffey AM; Waddell KW; Chekmenev EY Parahydrogen Induced Polarization of 1-^{13}C-Phospholactate-D_2 for Biomedical Imaging with >30,000,000-Fold NMR Signal Enhancement in Water. Anal. Chem 2014, 86, 5601–5605. [PubMed: 24738968]
68. Kharkov B; Duan X; Canary JW; Jerschow A Effect of Convection and B_1 Inhomogeneity on Singlet Relaxation Experiments. J. Magn. Reson 2017, 284, 1–7. [PubMed: 28926738]
69. Salnikov OG; Kovtunov KV; Barskiy DA; Bukhtiyarov VI; Kaptein R; Koptyug IV Kinetic Study of Propylene Hydrogenation over Pt/Al2O3 by Parahydrogen-Induced Polarization. Appl. Magn. Reson 2013, 44, 279–288.
70. Kiryutin AS; Pravdivtsev AN; Yurkovskaya AV; Vieth HM; Ivanov KL Nuclear Spin Singlet Order Selection by Adiabatically Ramped RF Fields. J. Phys. Chem. B 2016, 120, 11978–11986. [PubMed: 27786476]
71. Driehuys B; Cates GD; Miron E; Sauer K; Walter DK; Happer W High-Volume Production of Laser-Polarized Xe-129. Appl. Phys. Lett 1996, 69, 1668–1670.
72. Ruth U; Hof T; Schmidt J; Fick D; Jansch HJ Production of Nitrogen-Free, Hyperpolarized Xe-129 Gas. Appl. Phys. B-Lasers Opt 1999, 68, 93–97.

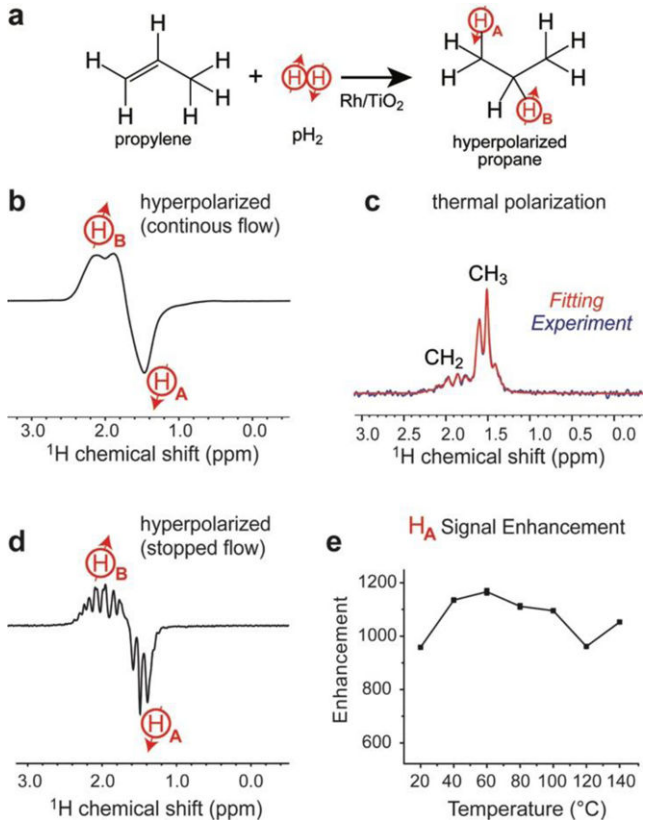

Figure 1.

^{1}H NMR single-scan spectroscopy of HP propane gas using the 1.4 T setup (see Scheme S1 for details). a) Schematic of heterogeneous pairwise pH_2 addition. b) ^{1}H NMR spectrum of HP propane acquired with the apparatus in continuous-flow mode. c) ^{1}H NMR spectrum of thermally polarized propane spectrum (blue) and spectral fitting (red) using the Bruker Daisy software package. d) ^{1}H NMR spectrum of HP propane acquired in a stopped-flow mode. e) Plot of NMR signal enhancement values of the HP methyl proton (H_A) at different operating temperatures obtained via continuous-flow operation (reactor prepared by mixing ~62 mg of the Rh/TiO_2 catalyst and 6.6 g of Cu in the 2nd stage of the hyperpolarizer). Connecting lines in display e) are meant only to guide the eye.

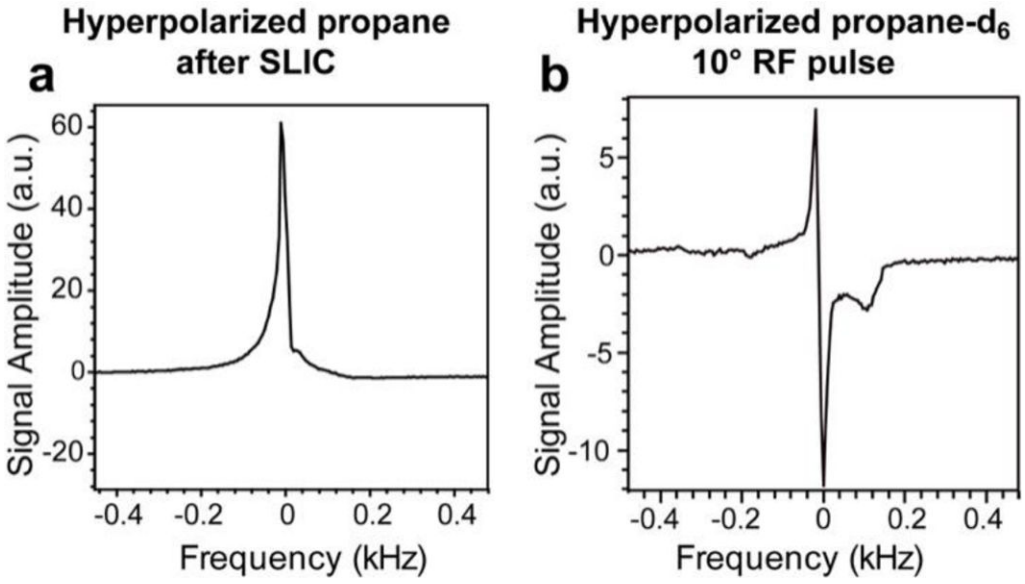

Figure 2.

a) ^{1}H 0.0475 T NMR spectrum of HP propane after SLIC transformation (as shown in Scheme 2b). b) ^{1}H 0.0475 T NMR spectrum of HP propane-d_6 acquired using a small-angle (~10°) hard RF pulse (as shown in Scheme 2e).

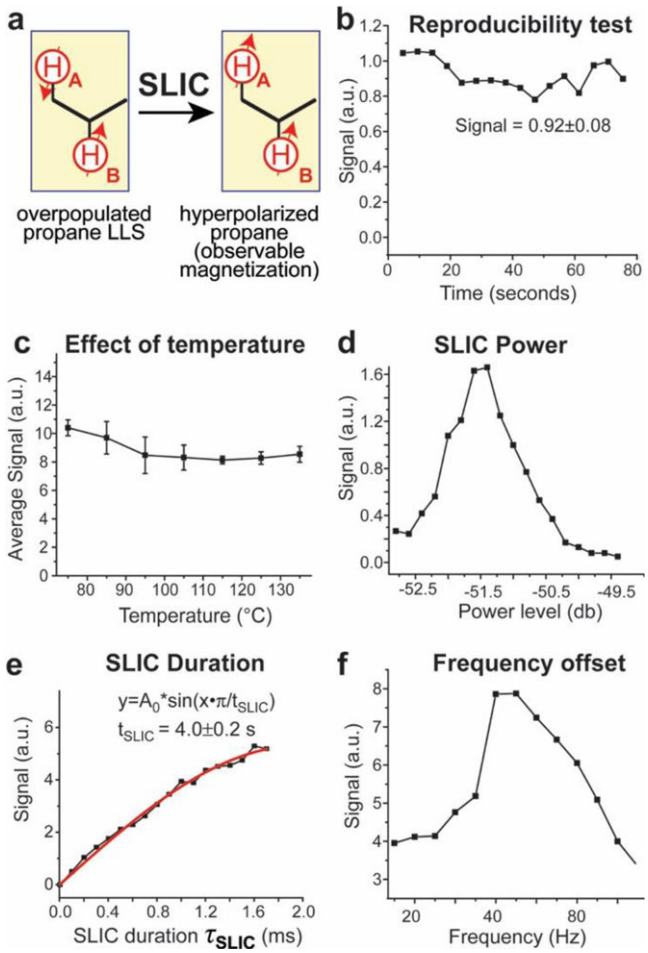

Figure 3.

Results from SLIC pulse optimization with HP propane data acquired using the 0.0475 T NMR spectrometer setup shown in Scheme 1 at production/reactor/reaction temperature of 60 ± 1 °C (except for display c) where the temperature was varied). a) Diagram showing the transformation of LLS of HP propane (denoted schematically as a singlet) into observable magnetization achieved using a SLIC pulse. b) Results from a test of the shot-to-shot reproducibility of the intensity of the HP propane signal. c) Temperature dependence of the average (over three data points) HP propane SLIC-induced signal using a 1:1 gas mixture of pH_2 and propylene. d) Optimization of RF power of the SLIC pulse (note the x-axis is provided in db units of the Kea NMR spectrometer due to the non-linearity of the RF amplifier at low power levels; the maximum is expected at B_1 RF strength between 10 Hz and 30 Hz[63]). e) The dependence of the HP propane signal on the SLIC pulse duration (experimental data: black points; a fit using a sinusoidal function is shown by the solid red curve). f) The dependence of the HP propane signal on the SLIC pulse frequency offset (the solid lines are added to guide the eye). Note a SLIC pulse duration of 500 ms was employed for the data acquisition in panels b), c), d), and f). Connecting lines in displays b), c), d), and f) are meant only to guide the eye.

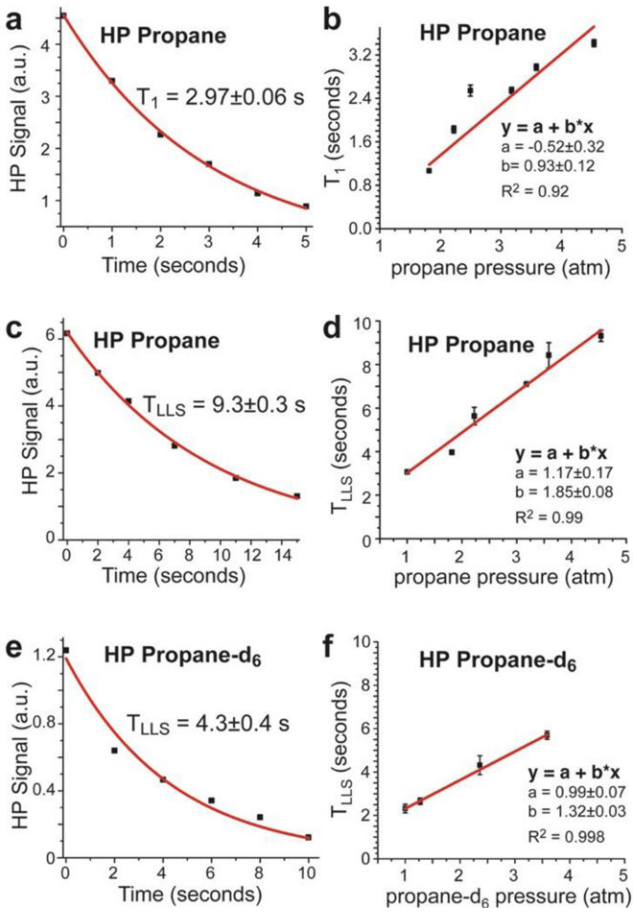

Figure 4.

Examples of T_1 (at ~3.6 atm pressure) and T_{LLS} (at ~4.5 atm pressure) signal decays of HP propane and mono-exponential fitting are shown in a) and c); e) shows a corresponding example of LLS decay of HP propane-d_6. Dependences of T_1 (b) and T_{LLS} (d) of propane hyperpolarization on its pressure. f) Dependence of T_{LLS} of propane-d_6 hyperpolarization on its pressure (an example of experimental data reporting on effective T_1 for HP propane-d_6 is shown in Figure S3). All data is acquired at 0.0475 T using production/reaction conditions of 75 °C and 2000 sccm flow rate with near-100% chemical conversion of pH_2 and unsaturated substrates. See Scheme 1 for additional details.

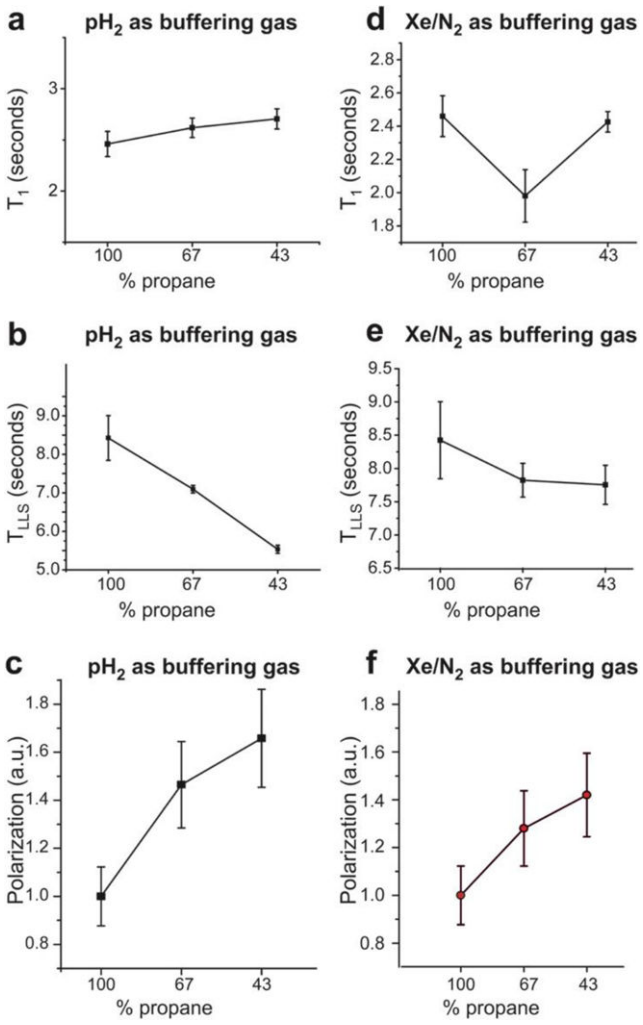

Figure 5.

Effects of using different buffering gases on the hyperpolarization decay constants and polarization levels of HP propane determined using the 0.0475 T magnetic field NMR spectrometer setup (Scheme 1). T_1 (a) and T_{LLS} (b) dependence of HP propane on the propane fraction in the resultant gas mixtures with the use of pH_2 buffering gas. c) Dependence of propane ^1H polarization (arbitrary units, a.u.) on the propane fraction in the resultant gas mixtures with the use of H_2 buffering gas. T_1 (d) and T_{LLS} (e) dependence of HP propane on the propane fraction in the resultant gas mixtures with the use of Xe/N_2 (3:1) buffering gas mixture. f) Dependence of propane ^1H polarization (arbitrary units, a.u.) on the propane fraction in the resultant gas mixtures with the use of Xe/N_2 (3:1) buffering gas mixture. All data were obtained at 38 psi backpressure (~3.6 atm total pressure), and the pH_2 to propylene ratio was 1:1 for the experiments shown in displays d, e, and f. Connecting lines are meant only to guide the eye.

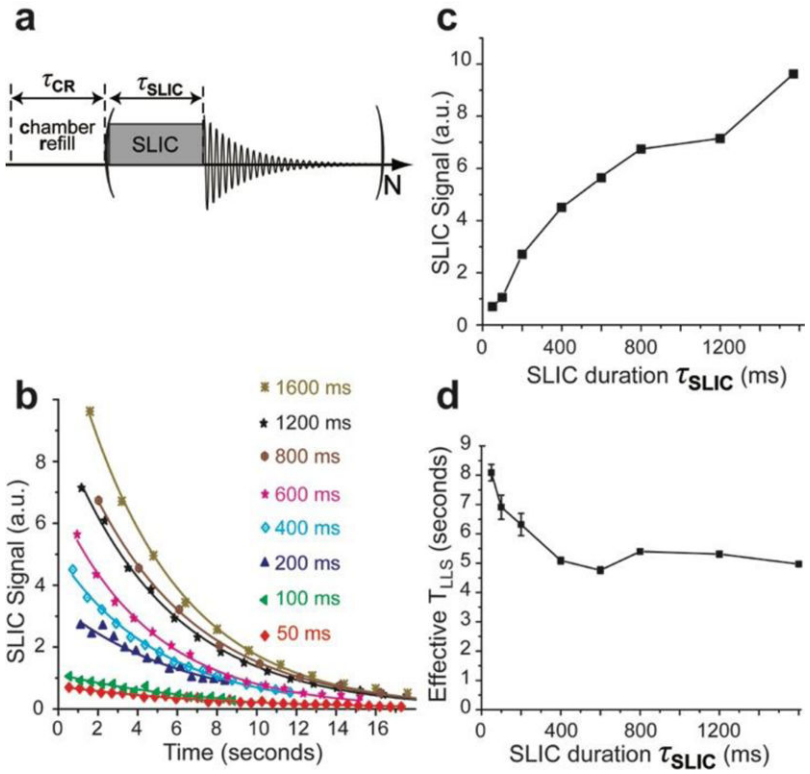

Figure 6.

a) Pulse sequence comprising a series of partial SLIC pulses with variable duration each followed by NMR signal acquisition; note the sequence is repeated *N* times on a single batch of static HP propane gas. b) The decay of HP propane signals obtained using the partial SLIC excitation scheme (with variable SLIC duration); note the color coding of the SLIC pulse duration in the figure legend (see Table S1 for additional details). c) The intensity of the first data point in display b) plotted as a function of the SLIC pulse duration. Connecting lines in displays c) and d) are meant only to guide the eye.

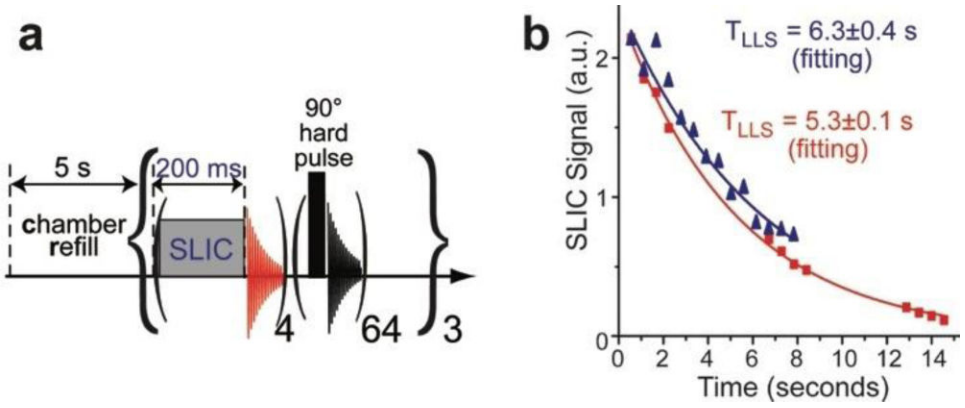

Figure 7.

a) Pulse sequence comprising a series of partial SLIC pulses with 200 ms duration followed by NMR signal acquisition. The 200 ms SLIC pulse is followed by NMR detection; this loop is repeated 4 times, and a train of sixty-four (equally spaced) hard 90° RF pulses is applied and the entire sequence is repeated three times. b) The recorded SLIC NMR signal intensities (comprising twelve data points). The mono-exponential fitting (red) yielded an effective T_{LLS} constant of 5.3±0.1 seconds. The corresponding decay curve without the use of hard RF pulses is shown by blue trace with triangles. All experiments were performed at 38 psi of overpressure (~3.6 atm total pressure).

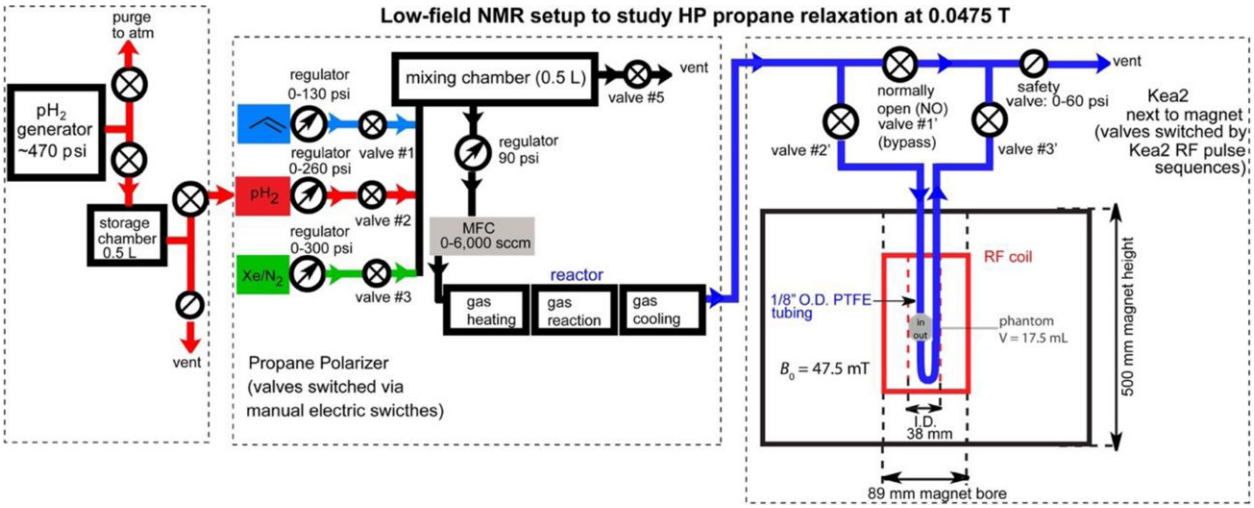

Scheme 1.

HET-PHIP polarizer apparatus and low-field NMR setup. This setup consists of three major components (outlined by dashed lines): parahydrogen generator, propane hyperpolarizer, and the 0.0475 T NMR spectrometer/pulse-programmable automated gas manifold controlled by Kea2 NMR spectrometer with a pressurized phantom (~17.5 mL).

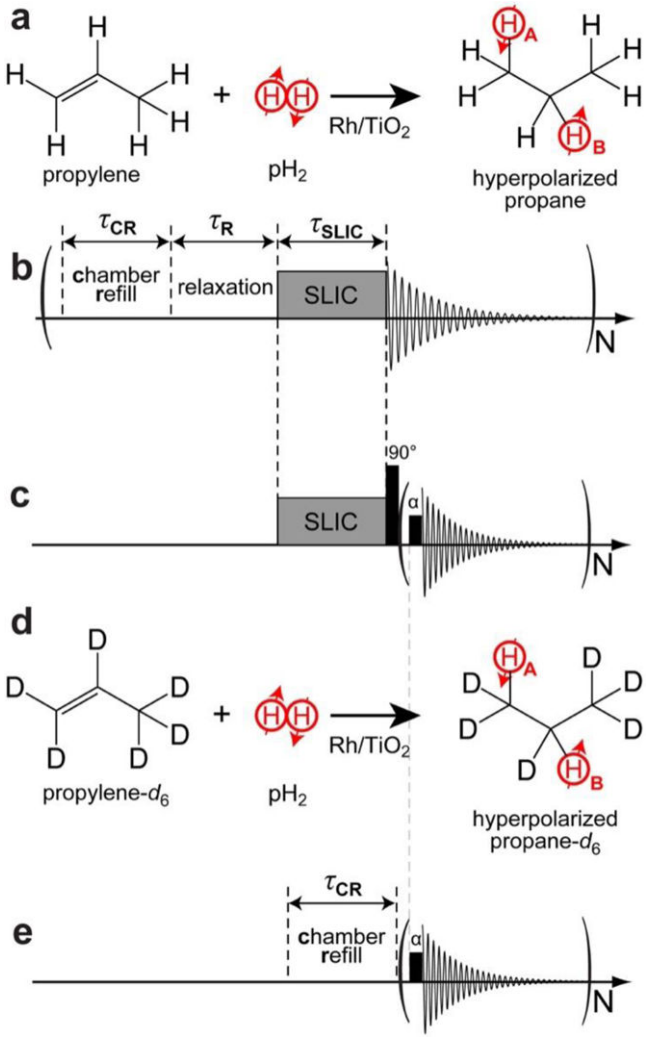

Scheme 2.

a) Diagram of the pairwise addition of pH_2 to propylene over the Rh/TiO_2 catalyst. b) the sequential steps of the signal acquisition method using the 0.0475 T setup for the measurement of HP propane T_{LLS} (achieved by varying the relaxation delay τ_R), optimization of the chamber-refill time τ_{CR}, and optimization of SLIC transformation (varying RF amplitude, power, and frequency offset). c) Corresponding pulse sequence used for HP propane T_1 measurements using 90° RF pulse (to create z-magnetization) after SLIC irradiation followed by a small angle (α) RF pulse; note the SLIC pulse and chamber refill are performed once in the sequence shown in c) versus multiple refills employed in sequence shown in b). d) Diagram of the pairwise addition of pH_2 to propylene-d_6 over the Rh/TiO_2 catalyst. e) Pulse sequence used for the measurement of HP propane-d_6 T_{LLS}. Note the pH_2 symmetry breaking is achieved by the chemical reaction, with nascent protons H_A and H_B placed in methylene and methyl chemical groups in a) and d).